PERFORMANCE OF LARGE AREA XENON ION THRUSTERS FOR ORBIT TRANSFER MISSIONS

Vincent K. Rawlin
National Aeronautics and Space Administration
Lewis Research Center
Cleveland, Ohio 44135

ABSTRACT

Studies have indicated that xenon ion propulsion systems can enable the use of smaller Earth-launch vehicles for satellite placement which results in significant cost savings. These analyses have assumed the availability of advanced, high power ion thrusters operating at about 10 kW or higher. A program was initiated to explore the viability of operating 50 cm diameter ion thrusters at this power level. Operation with several discharge chamber and ion extraction grid set combinations has been demonstrated and data were obtained at power levels to 16 kW. Fifty cm diameter thrusters using state of the art 30 cm diameter grids or advanced technology 50 cm diameter grids allow discharge power and beam current densities commensurate with long life at power levels up to 10 kW. In addition, 50 cm diameter thrusters are shown to have the potential for growth in thrust and power levels beyond 10 kW.

INTRODUCTION

Recent studies have quantified the economic and deployment time benefits of using high specific impulse xenon ion propulsion systems to place a constellation of satellites in operational orbit.[1,2] Ion propulsion can, in some cases, allow the use of a smaller and less expensive Earth-launch vehicle.[1] This approach leads to significant reductions in cost to deploy a constellation of satellites. In addition, the constellation deployment time may be reduced with multiple payloads and/or a higher launch frequency using the smaller launch vehicles.[1]

Ion propulsion components and systems have been ground and flight tested worldwide for three decades.[3-11] Ion propulsion, using propellants such as mercury, cesium, xenon, and argon, have been developed for auxiliary propulsion needs, such as stationkeeping and for primary propulsion of Earth-orbit and planetary transfer vehicles. Mercury ion thrusters with diameters of 50 cm[12] and 150 cm[13] were tested at beam power levels of about 20 and 200 kW, respectively, more than 20 years ago. Due to space power restrictions, however, most subsequent ion thruster research has been conducted at power levels under 5 kW. But, with the advent of large solar power systems of the Space Station Freedom, advanced photovoltaic solar arrays[14] and nuclear reactor systems such as SP-100,[15] the opportunities for utilization of primary ion propulsion are increasing.

Propulsion systems of a few tens of kW offer major benefits for orbit transfer missions.[1,2] Xenon ion thrusters, at about 10 kW, appear optimum when the number of devices and reliability issues are considered.[2]

The 3 kW, 30 cm diameter divergent magnetic field mercury ion thruster, developed in the 1970's for the Solar Electric Propulsion System[5] was converted to operate with inert gases[16] and has been tested extensively at power levels to 10 kW.[17] Reference 17 presented erosion rates of internal components for that thruster. Anticipated problems were solved with geometric and operating point changes, but, at an input power level of 10 kW, erosion of the discharge baffle was so severe that research on 30 cm diameter divergent field thrusters has been terminated at NASA's Lewis Research Center (LeRC). A variation of the ring-cusp boundary magnetic field discharge chamber geometry,[18] which does not require a discharge baffle, is now the baseline design. Thrusters of this geometry have been evaluated with inert gas and mercury propellants[7,18-22] over a wide range of power levels and for periods in excess of 4300 hr.[7]

There are known limits to gridded, high power ring-cusp ion thrusters. Two major ones are: (1) maximum beam current density and (2) maximum thruster component temperatures. The maximum beam current density and, therefore, the maximum thrust density of electrostatic ion thrusters are strong functions of specific impulse. Thus, large area thrusters are required for high values of thrust at relevant values of specific impulse. Rare-Earth permanent magnets are critical components of ring-cusp ion thrusters. Degradation of magnetic field strengths limit the magnet temperature to about 300 °C which places an upper bound on discharge chamber power density. Thermal margins should increase with thruster size for a fixed discharge power.

Preliminary performance data of two 50 cm diameter discharge chambers, evaluated with one set of 50 cm diameter ion extraction grids, have been presented.[21] This paper presents additional performance characteristics of the 50 cm diameter ring-cusp thruster evaluated with a 30 cm diameter grid set and three different 50 cm diameter ion extraction grid sets.

APPARATUS

The performance of several ion thruster configurations was evaluated over a range of operating conditions with xenon propellant. The experimental hardware and support equipment are described.

DISCHARGE CHAMBERS

Figure 1 shows section views of the 50 cm diameter ring-cusp discharge chamber. The mild steel shell was lined with rings of rare-Earth samarium cobalt magnets ($SmCo_5$) to produce strong boundary magnetic fields which contained the discharge plasma more efficiently than other geometries.[18,19] The spacings between magnet rings was initially chosen to be nearly the same as those found to be optimum by Sovey in Ref. 18. Figure 1(b) also shows a grid set adapter plate which was required when 30 cm diameter grids were used. The adapter plate, which was electrically isolated from the discharge chamber, had either 0, 1, or 2 layers of magnets arranged in three rings. These configurations were designated "RC0", "RC1", and "RC2", respectively. Figure 1(b) shows the three rings with 2 layers of magnets. The 29.6 cm diameter by 7.5 cm long cylindrical section of the adapter plate was insulated from the discharge plasma with a layer of polyimide film.

ION EXTRACTION GRID SETS

Four sets of dished two-grid ion extraction systems were used in this investigation and are described in Table 1. General fabrication methods for dished grids were described in Ref. 23. Grid mounting techniques were described in Ref. 21.

Grid set 1 was nominally 30 cm in diameter while the others all had diameters of 50 cm. The accelerator grid hole diameters for 50 cm diameter grids varied from 1.91 mm to 1.52 and 1.14 mm to reduce neutral propellant losses. The 50 cm diameter screen grids were electrically isolated from the discharge chamber and could be biased to allow measurement of ion currents.

VACUUM FACILITY

Thruster evaluation was conducted in a 4.6 m diameter by 19.2 m long vacuum facility at LeRC. The actual working length was halved by a full diameter mid-tank baffle. Vacuum facility pressure without propellant flow was about 1×10^{-4} Pa (8×10^{-7} torr) which was achieved with twenty 0.8-m diameter silicon oil diffusion pumps. For xenon flow rates of 3 to 12×10^{-6} kg/s the facility pressures, during thruster operation, varied from about 0.5 to 2.0×10^{-3} Pa (0.4 to 1.6×10^{-5} torr). The pressure was measured about 6.4 m from the thruster ion extraction grids.

PROPELLANT SUPPLY

High purity (99.995 percent pure), research grade xenon propellant was supplied to the cathode and discharge propellant feed lines through flowmeters and flow controllers. The flowmeters utilized heated capillary tubes and flowing gas to sense relative heat transfer. The gas flow rates were controlled by using piezoelectric leak valves actuated by an error signal generated by the difference between the flowmeter output and a reference signal. For initial operating convenience, the flow controllers were located near the power supply controls and about 8 m from the thruster. The long cathode propellant line length and a cathode orifice flow impedance dependency on cathode emission current made it difficult to precisely control low cathode flow rates. There was no problem with the main propellant flow rate because the main propellant line opened directly to the low pressure discharge chamber. The propellant flow rates were expressed as equivalent currents of singly-charged ions. Typical cathode and main propellant flow rate ranges were 0.1 to 0.7 eq.A. and 2 to 8 eq.A., respectively.

POWER SUPPLIES

Thruster power was provided by 60 Hz laboratory power supplies. Figure 2 shows a schematic of the power supplies and typical output values. The maximum output of the beam power supply was 20 A at 2000 V. The maximum discharge current was 93 A. Additional power supply information is given in Ref. 16.

PROCEDURE

The thruster was installed in the vacuum facility and the discharge cathode and neutralizer cathode feed lines were purged. The cathode was heated slowly to about 1100 °C and 1000 V was applied to the starting electrode. A main discharge flow rate ($\dot{m}_M$) of about 2 eq.A. (3×10^{-6} kg/s) was applied and the cathode flow rate ($\dot{m}_C$) was raised to about 3.4 eq.A. (5×10^{-6} kg/s) to initiate the plasma discharge. The cathode flow rate was then reduced to achieve steady-state conditions. Positive and negative high voltages were applied to the screen and accelerator grids, respectively, to extract an ion beam.

The discharge chamber was characterized with beam extraction by varying the discharge current (J_D) at constant propellant flow rates. A beam ion production cost (EV) was calculated as follows:

$$EV = \frac{VD(J_D - J_B)}{J_B} \tag{1}$$

and plotted as functions of the discharge propellant efficiency.

$$\eta D = \frac{J_B}{\dot{m}_M + \dot{m}_C + \dot{m}_I} \tag{2}$$

Some propellant ($\dot{m}_I$) is ingested from the facility through the accelerator grid holes and is estimated from

$$\dot{m}_I = \frac{p_F A_O K_C e}{4} \sqrt{\frac{8}{\pi k T_w m}} \quad , \text{eq.A.} \tag{3}$$

where P_F is the true facility pressure, A_O is the accelerator grid open area, and K_C is a Clausing conductance factor[24] for the accelerator grid hole geometry. All the symbols are defined in the symbol list. Equation (3) assumes free molecular flow through the accelerator grid holes into the discharge chamber. The ingested xenon atoms were assumed to have a mean velocity based on a vacuum facility wall temperature of 300 K. Table 2 lists the ingested flow equations used for each grid geometry. As an example, values of $\dot{m}_I$ at a background pressure of 1.33×10^{-3} Pa (1×10^{-5} torr) ranged from 0.04 eq.A. for grid set 1 to 0.29 eq.A. for grid set 2. During thruster operation the background gas was primarily xenon because the base pressure was about 1×10^{-4} Pa.

Ion currents to the screen grid (J_S) and adapter plate were measured by applying a negative bias to those surfaces to repel discharge electrons. Normal thruster operation was conducted without using the bias supplies. The beam current (J_B) and accelerator grid impingement current (J_A) were measured as functions of thruster geometry and operating conditions.

Under most operating conditions some discharge chamber propellant is doubly-ionized leading to high, uncorrected propellant efficiencies. Doubly-ionized xenon contents have not been measured for any 50 cm diameter thruster. Therefore, measured propellant efficiencies were used in discharge chamber performance discussions. However, when thrust, specific impulse, and thruster efficiency values for the 50 cm diameter thrusters were calculated, a thrust correction factor which accounts for doubly-charged atoms was used. The production of doubly-charged propellant was found to be primarily a function of the measured propellant efficiency.[16,18,25] The thrust correction factor for multiply charged propellant (α) was calculated using Fig. 1 of Ref. 16, which gives values of the ratio of doubly-to-singly charged ion currents (r), for several 30 cm diameter thrusters, as functions of the measured propellant efficiency. The curve for the 30 cm diameter ring-cusp thruster was used with measured propellant efficiencies of the 50 cm diameter discharge chamber to calculate multiply charged ion thrust correction factors.

For all thruster tests presented herein, the high voltage common was grounded to the vacuum facility and beam neutralizing electrons were emitted from the vacuum facility walls and mid-tank baffle as a result of energetic ion impingement. When a neutralizer was used with 50 cm diameter thrusters,[21] minimum xenon propellant flow rates required were found to be about 6 percent of the beam current. Therefore, calculated values of specific impulse and thruster efficiency include a value for $\dot{m}_N$ which is 6 percent of the beam current.

Additional assumptions were made before overall thruster performance parameters were calculated. The neutralizer to ground floating voltage (V_G) was assumed to be equal to the discharge voltage (V_D). This made the net accelerating voltage (V_N) equal to the output voltage of the beam power supply (V_B). A constant fixed power loss of 200 W was assumed to account for cathode and neutralizer keeper powers and accelerator grid impingement losses. A thrust correction factor (F_T) which accounts for nonaxial ion trajectories was estimated to be 0.98 for all data presented.[16] The following equations were used to calculate the overall xenon thruster efficiency:

$$V_N = V_B + V_D - V_G \approx V_B \tag{4}$$

$$P = J_B(V_N + EV) + 200 \tag{5}$$

$$T = \gamma J_B \sqrt{\frac{2mV_N}{e}} \tag{6}$$

$$I_{sp} = \frac{\gamma T}{\dot{m}_T g} \tag{7}$$

$$\eta_T = \frac{\gamma^2 g T I_{sp}}{2P} \tag{8}$$

RESULTS

The performance of a 50 cm diameter ring-cusp discharge chamber was characterized with 30 and 50 cm diameter ion extraction grids. Values of overall thruster performance were also calculated.

DISCHARGE CHAMBER PERFORMANCE

Figure 3 shows the beam ion production cost (EV) as functions of the discharge chamber propellant efficiency (η_D) for some of the data taken. The levels of performance shown for each configuration varied only slightly for propellant flow rates up to 50 percent above and below those presented.

30 cm diameter grids - The upper 3 curves of Fig. 3 give typical performance of the 50 cm diameter ring-cusp discharge chamber with 30 cm diameter grids and different adapter plate magnetic configurations. At a fixed propellant efficiency of 0.8, values of EV decreased from 385 to 235 W/A as the flux density at the adapter plate magnet cusps was increased. This performance improvement occurred because the ion current reaching the screen grid and the adapter plate was reduced, as shown in Fig. 4, when the adapter plate magnet cusp flux density was increased. With no adapter plate magnets the unextracted ion current at the grid plane was about 7 A. When 1 and 2 layers of magnets were added, this current dropped to 2.1 and 1.6 A, respectively. For the 1-layer case, the adapter plate and screen grid currents were monitored separately. The ratio of screen grid current to beam current was found to be about 0.33±0.05 over a wide range of operating conditions. Based on the fact that a single grid set was used for all three cases, about 1.1 A of ion current was assumed to be collected by the screen grid for the conditions of Fig. 4. With this assumption, the adapter plate ion current decreased from about 6 A to only 0.5 A as the cusp flux density was increased from 0 to 0.36 torr. With fewer ions lost to the adapter plate, less discharge power was required to produce the same ion beam current. While the adapter plate ion losses were significantly reduced, the decrease in EV was not as dramatic because other discharge power loss mechanisms existed. Also, the addition of magnets to the adapter plate may have reduced the effective discharge chamber ionization volume. This ability of strong cusp magnetic fields to control plasma wall losses is the primary advantage of ring-cusp thrusters.

Another observation from Fig. 3 is the range of values of discharge voltage for the data shown. The discharge voltage can be used to trade discharge chamber performance with lifetime limited by thruster internal erosion.[16] Higher values of discharge voltage are desirable for greater ionization efficiencies, but unextracted ions, such as those striking the screen grid, do sputtering damage. Therefore, lower values of discharge voltage are required for reduced thruster internal erosion. Reference 17 has shown that acceptable screen grid erosion rates, consistent with 10 000 hr lifetime, were achieved with a 10 kW, 30 cm diameter xenon ion thruster when the discharge voltage was 28 V. When 30 cm diameter grids (grid set 1) were used on the 50 cm diameter discharge chamber, the effective open area fraction was only about 8 percent. Therefore, the neutral density was higher and values of discharge voltage lower than normal (28 V) were obtained for normal values of $\dot{m}_c$ (0.2 to 0.3 eq.A). Discharge chamber operation at discharge voltages of 23 or 24 V provide relatively low sputter erosion of cathode potential surfaces. Operation at these cathode flow rates also provided a more stable discharge and reliable high-voltage recycle sequences.

50 cm diameter grids - When 50 cm diameter grids were used, values of EV were reduced to as low as 100 W/A. This improvement may be seen in Fig. 3 by comparing the performance values of similar discharge chambers and different size grids. For example, the best performance of the RCO case indicated 10.3 A of ions reached the grid plane at a propellant efficiency of 0.8, but only 3 A, or one-third of the ions, were extracted. When grid set 4, which had nearly 3 times the extraction area of grid set 1, was used nearly all of the ions reaching the grid plane were extracted. The 50 cm diameter discharge chamber required 3.8 times less discharge power, to produce the same beam current and propellant efficiency, with grid set 4 as with grid set 1. The major reason for this improved performance is believed to be that ions produced, but not extracted with 30 cm diameter grids, were accelerated as beam ions with 50 cm diameter grids.

Values of EV for 50 cm diameter grids (sets 2 to 4) decreased (Fig. 3) with decreasing accelerator grid hole diameter. The reason for this is that the neutral propellant atom losses through the grid set were reduced with smaller grid holes which led to an increase in the neutral density. At a fixed discharge power the beam current typically increases with increasing neutral density yielding a reduced value of EV. This effect has been observed with smaller thrusters.[26,27]

From a discharge chamber performance viewpoint, grid set 4 would be the preferred geometry as it was for 30 cm diameter thrusters.[5] But, poor ion extraction capability of grid set 4 necessitated high total grid voltages, which led to failure of the mica insulator used to set the spacing at the edge of the grids. These failures prevented the acquisition of data at propellant efficiencies of interest, as shown in Fig. 3.

Values of discharge voltage were high for all three 50 cm diameter grid sets when the discharge chamber was operated at low propellant flow rates (Fig. 3) due to increased neutral losses compared to that with 30 cm diameter grids. The effective accelerator grid open areas for 50 cm diameter grids were 2.4 to 7.5 times greater than that of the 30 cm diameter grids. Significant increases in propellant flow rate and discharge power for grid sets 2 and 3 resulted in values of discharge voltage commensurate with low internal erosion rates in high power xenon thrusters.

In summary, the 50 cm diameter ring-cusp discharge chamber was characterized with 30 and 50 cm diameter grids. When 30 cm diameter grids were utilized, the minimum beam ion production costs were initially very high at 385 W/A but decreased to about 230 W/A with the addition of magnet rings to the cathode potential adapter plate which drastically reduced the ion losses to that surface. When 50 cm diameter grids replaced the 30 cm diameter grids and magnet-free adapter plate, the beam ion production costs decreased from 385 to 100 W/A, at a propellant efficiency of 0.8, for grids with small accelerator holes. The reduction of beam ion production costs occurred because ions which impinged on the adapter plate were extracted when full size 50 cm diameter grids were used. Comparing only 50 cm diameter grids at a propellant efficiency of 0.8, the beam ion production costs decreased from 155 W/A, for the grid set with largest accelerator holes, to 100 W/A for the grid set with the smallest accelerator holes. This effect was caused by a reduction of the neutral atom losses through the accelerator grid which, at constant inlet flow rates and discharge power, led to beam current increases and reduced beam ion production costs. Efficient operation with the ring-cusp discharge chamber was possible at low values of discharge voltage which should lead to internal erosion rates comparable to or lower than those obtained in recent lifetests at 28 V.

OVERALL THRUSTER PERFORMANCE

Values of input power, thrust, specific impulse, and efficiency were calculated for the 50 cm diameter ring-cusp thruster using demonstrated discharge chamber and grid set operating conditions. Table 3 lists the operating conditions and results for the four grid sets tested. Figures 5 and 6 show the thrust obtained as a function of thruster input power and thruster efficiency as a function of specific impulse, respectively.

Figure 5 shows that the values of thrust achieved with two-grid 30 and 50 cm diameter grids increased from 0.1 to 0.5 N as the thruster input power was varied from 2.4 to 16 kW. Thrust to power ratios decreased from about 0.04 to 0.03 N/kW as discharge chamber conditions and grid voltages were increased over wide ranges as shown in Table 3. The thrust to power ratios are insensitive to thruster operating conditions when the net accelerating voltage is much greater than the ion production cost as seen from Eqs. (5) and (6). When this condition exists, most of the thruster power is in the beam, so, large changes in the ion production cost cause minor changes in the thrust to power ratio.

Figure 6 and Table 3 show that ion thruster efficiency ranged from about 0.4 to 0.8 as the specific impulse was increased from 2200 to 5100 sec. Thruster efficiency was found to be nearly specified by only the specific impulse. This occurs, as seen from Eq. (8), when the thrust to power ratio is constant (as in Fig. 5). Algebraic manipulation of Eqs. (4) to (8) shows that thruster efficiency is approximately proportional to the net accelerating voltage divided by the sum of the net accelerating voltage and ion production cost. Thus, thruster efficiency is expected to increase with specific impulse as the ion production cost becomes negligible when compared to the net accelerating voltage.

In addition to thruster performance, all 4 thruster geometries have shown the possibility of efficient operation at low values of discharge voltage. This should reduce thruster internal erosion. A 50 cm diameter discharge chamber with well-developed state of the art 30 cm diameter grids is an attractive configuration for a 10 kW-class xenon ion thruster. Operation at high values of beam current and propellant efficiency have been demonstrated. The high propellant efficiency should reduce the accelerator grid charge exchange damage that was reported in Ref. 17. The increased electron collection area of the 50 cm diameter discharge chamber should provide an environment for the rare-Earth magnets with greater thermal margin than that of smaller discharge chambers. Operation with 50 cm diameter grids has the potential of significantly reducing screen and accelerator grid erosion because the average current densities should be nearly a factor of 3 less than those of thrusters with 30 cm diameter grids operating at comparable power levels.

CONCLUSIONS

Opportunities exist for high power, high specific impulse xenon ion thrusters. Large diameter thrusters operating at derated conditions offer prospects for improved lifetime and a modest discharge chamber thermal environment compared to smaller thrusters. Therefore, a 50 cm diameter ring-cusp xenon ion thruster was operated with 30 and 50 cm diameter dished two-grid ion extraction grids. The thrust was found to increase nearly linearly from 0.1 to 0.5 N as the power was increased from 2.4 to 16 kW. For these data the specific impulse varied from about 2200 to 5100 sec and specified the thruster efficiency, which varied from 0.4 to 0.8.

The minimum beam ion production cost of the 50 cm diameter discharge chamber with 30 cm diameter grids ranged from 385 to 230 W per beam ampere as the magnetic geometry of the grid adapter plate was varied. These costs decreased further when 50 cm diameter grids were used because ions formed beyond the 30 cm diameter were extracted and not lost to the discharge chamber walls. With 50 cm diameter grids, the minimum beam ion production costs dropped from 155 to 100 W/A as the accelerator grid hole diameters were decreased because the discharge chamber neutral density increased.

From the data presented, two geometric alternatives to the baseline 30 cm diameter thruster exist for operation at 10 kW. The 50 cm diameter discharge chamber with 30 cm diameter grids offers several potential benefits, which include: (1) the use of well-developed state of the art ion extraction grids as a near-term option, (2) potentially low internal erosion due to low values of discharge voltages, (3) cooler thermal environment for rare-Earth magnets, (4) and high propellant efficiency for reduced accelerator grid charge exchange erosion. The other option would be to use 50 cm diameter grids to obtain reduced values of beam current density which would lead to reduced internal erosion rates. With more efficient ion production, the discharge power density would also be reduced which should increase the thermal margin for the rare-Earth magnets. As 50 cm diameter ion extraction grid fabrication and mounting procedures are improved, 50 cm diameter thrusters would also have a significant potential for growth in thrust and power levels beyond 10 kW.

SYMBOLS

A_O accelerator grid open area, m^2

d_A accelerator grid hole diameter, mm

EV beam ion production cost, W/A

e electronic charge, 1.6×10^{-19} C

F_T thrust reduction factor due to ion beam divergence

g acceleration of gravity, 9.81 m/s^2

Isp specific impulse, s

J_A accelerator grid impingement current, A

J_B ion beam current, A

J_D discharge current to anode, A

J_S screen grid ion current, A

K_C Clausing conductance factor

k Boltzmann's constant, 1.38×10^{-23}, J K^{-1}

m xenon atom mass, 2.18×10^{-25} kg

$\dot{m}_C$ discharge cathode flow rate, eq.A.

$\dot{m}_I$ ingested flow rate, eq.A.

$\dot{m}_M$ discharge main flow rate, eq.A.

$\dot{m}_N$ neutralizer cathode flow rate, eq.A.

$\dot{m}_T$ total propellant flow rate, $(\dot{m}_C+\dot{m}_I+\dot{m}_M+\dot{m}_N)$ m/e, kg/s

P thruster input power, W

P_F vacuum facility pressure, Pa

r ratio of doubly-to-singly charged ion currents

T thrust, N

T_W vacuum facility wall temperature, K

V_A accelerator grid voltage, V

V_B screen grid voltage, V

V_D discharge voltage, cathode to anode potential, V

V_G neutralizer-to-ground potential, V

V_N net accelerating voltage, $V_N = V_B + V_D - V_G$, V

α thrust correction factor due to multiply - charged ions, $= \frac{1 + \frac{\sqrt{2}}{2} r}{1 + r}$

γ total thrust correction factor, $\gamma = \alpha F_T$

η_D discharge propellant efficiency, uncorrcted for multiply charged ions, $\frac{J_B}{m_C + m_I + m_M}$

η_P total thruster propellant efficiency uncorrected for multiply charged ions, $\frac{J_B}{m_C + m_I + m_M + m_N}$

η_T overall thruster efficiency

REFERENCES

1. Deininger, W.D., and Vondra, R.J., "Electric Propulsion for Constellation Deployment and Spacecraft Maneuvering," AIAA 88-2833, July 1988.

2. Sponable, J.M., and Penn, J.P., "An Electric Orbital Transfer Vehicle for Delivery of NAVSTAR Satellites," AIAA Paper 87-0985, May 1987.

3. Cybulski, R.J., et al., "Results From SERT I Ion Rocket Flight Test," NASA TND 2718, March 1965.

4. Kerslake, W.R., Goldman, R.G., and Nieberding, W.C., "SERT II: Mission, Thruster Performance, and In-Flight Thrust Measurement," Journal of Spacecraft and Rockets, Vol. 8, No. 3, March 1971

5. "The 30 cm Ion Thrust Subsystem Design Manual," NASA TM-79191, 1979.

6. Power, J.L., "Planned Flight Test of a Mercury Ion Auxiliary Propulsion System I - Objectives, Systems Descriptions, and Mission Operations," AIAA Paper 78-647-1, American Institute of Aeronautics and Astronautics (1978). (NASA TM-78859)

7. Beattie, J.R., Matossian, J.N., and Robson, R.R., "Status of Xenon Ion Propulsion Technology," AIAA Paper 87-1003, May 1987.

8. Nakamura, Y., et al., "Flight Performance of 5 cm Mercury Ion Thrusters on Engineering Test Satellite III," IEPC Paper 84-19, May 1984.

9. Shimada, S., Sato, K., Takegahara, H., and Kajiwara, K., "20 mN Class Xenon Ion Thruster for ETS-VI," AIAA Paper 87-1029, May 1987.

10. Schreib, R., "Electric Propulsion: Implementation Issues." IEPC Paper 88-006, October 1988.

11. Berry, W., Bartoli, C., and Trippi, A., "The ESA Policy and Programme for Development of Electric Propulsion," IEPC Paper 88-001, October 1988.

12. Reader P.D., "Experimental Performance of a 50 Centimeter Diameter Electron-Bombardment Ion Rocket," AIAA Paper 64-689, August-September 1964.

13. Nakanishi, S., and Pawlik, E.V., "Experimental Investigation of a 1.5 m Diameter Kaufman Thruster," AIAA Paper 67-725, September 1967.

14. Kurland, R., and Stella, P., "Status of Advanced Photovoltaic Solar Array Program," IECEC Paper 88-9050, July 1988.

15. Wiley, R.L., et al.: Space Reactor Power 1986: A Year of Choices and Transition. 21st Intersociety Energy Conversion Engineering Conference, Advancing Toward Technology Breakout in Energy Conversion, Vol. 3, American Chemical Society, 1986, pp. 1411-1415.

16. Rawlin, V.K., "Operation of the J-Series Thruster Using Inert Gas," AIAA Paper 82-1929, November 1982.

17. Rawlin, V.K., "Internal Erosion Rates of a 10 kW Xenon Ion Thruster," AIAA Paper 88-2912, July 1988.

18. Sovey, J.S., "Improved Ion Containment Using a Ring-Cusp Ion Thruster," Journal of Spacecraft and Rockets, 21, No. 5, September-October 1984, pp. 488-495.

19. Beattie, J.R., and Poeschel, R.L., "Ring-Cusp Ion Thrusters," IEPC Paper 84-71, May 1984.

20. Patterson, M.J., "Performance Characteristics of Ring-Cusp Thrusters with Xenon Propellant," AIAA Paper 86-1392, June 1986.

21. Patterson, M.J., and Rawlin, V.K., "Performance of 10 kW Class Xenon Ion Thrusters," AIAA Paper 88-2914, July 1988.

22. Yamagiwa, Y., et al., "A 30 cm Diameter Xenon Ion Thruster - Design and Initial Test Results," IEPC Paper 88-095, October 1988.

23. Rawlin, V.K., Banks, B.A., and Byers, D.C., "Design, Fabrication, and Operation of Dished Accelerator grids on a 30-cm Ion Thruster," Journal of Spacecraft and Rockets, Vol. 10, No. 1, January 1973, pp 29-35.

24. Clausing, P., "Uber die Stromung sehr verdunnter Gase durch Rohren von beliebiger Lange," Annalen
der Physik, Vol. 12, pp. 961-989, 1932.

25. Vahrenkamp, R.P, "Characteristics of a 30-cm Thruster Operated with a Small Hole Accelerator Grid Ion Optics," AIAA Paper 76-1030, November 1976.

26. Rawlin, V.K., "Sensitivity of 30 cm Mercury Bombardment Ion Thruster Characteristics to Accelerator Grid Design," AIAA Paper 78-668, April 1978. (NASA TM-78861)

27. Hudson, W.R., and Banks, B.A., "High-Performance Auxiliary Propulsion Ion Thruster with Ion-Machined Accelerator Grid," NASA TM X-3155, January 1975.

TABLE I. - DIMENSIONS OF ION EXTRACTION GRIDS

Grid set	Active diameter, cm	Dish depth, cm	Screen grid[a]			Accelerator grid		Grid spacing		
			Thickness, mm	Hole diameter, mm	Open area fraction	Thickness, mm	Hole diameter, mm	Open area fraction	Center, mm	Edge, mm
1	28.7	2.5	0.38	1.91	0.67	0.51	1.27	0.30	0.76	0.55
2	49	4.4	.38	1.91	.67	.38	1.91	.67	.81	.66 to 1.0
3	49	5.2	.38	1.91	.67	.38	1.52	.43	.76	.56 to 1.0
4	49	4.8	.38	1.91	.67	.38	1.14	.24	.66	.38 to .66

[a]All hole pattern dimensions reduced 0.2 percent to reduce hole misalignment due to dishing and finite grid thickness.

TABLE 2. - INGESTED XENON FLOW RATES, $\dot{m}_I$

Grid set	Accelerator grid open area, A_o, m^2	Clausing factor, K_c	$\dot{m}_I$ =
1	0.0194	0.72	30 P_F
2	.126	.83	220 P_F
3	.0811	.80	140 P_F
4	.0453	.75	72 P_F

TABLE 3. - OVERALL 50 CM DIAMETER XENON THRUSTER PERFORMANCE

Grid set	J_B, A	V_N, V	V_D, V	EV, W/A	η_D	η_P	α	γ	P, W	T, N	I_{sp}, s	η_T
1	2.38	1000	22.1	241	1.05	0.988	0.964	0.945	3150	0.117	3660	0.666
	3.15	1210	24.5	240	1.02	.962	.971	.952	4770	.172	3940	.696
	4.10	1380	22.0	250	.990	.934	.978	.958	6880	.241	4120	.707
	5.06	1500	22.4	260	1.06	.993	.962	.943	9110	.305	4490	.737
	5.74	1600	21.8	245	1.00	.940	.976	.956	10800	.362	4450	.731
	7.70	1810	23.0	257	1.13	1.06	.938	.919	16100	.497	5130	.776
2	2.37	803	30.9	143	.654	0.629	0.997	0.977	2440	0.108	2160	0.468
	3.16	830	31.0	165	.875	.831	.990	.970	3340	.146	2870	.615
	3.63	1300	32.0	165	1.01	.948	.975	.956	5520	.206	4050	.741
	4.58	1300	29.5	131	.839	.799	.992	.972	6750	.265	3470	.668
3	1.92	1030	32.0	151	.840	0.800	0.992	0.972	2470	0.099	3090	0.607
	3.15	1440	32.2	133	.909	.862	.987	.967	5150	.191	3920	.712
	3.80	1800	30.2	164	1.09	1.02	.953	.934	7660	.248	5000	.793
	5.00	2000	25	136	.807	.770	.993	.973	10900	.359	4150	.670
	5.96	2100	29	129	.965	.912	.981	.961	13500	.433	4970	.781
	6.46	2200	24	126	.788	.752	.994	.974	15200	.487	4250	.667
4	2.09	1535	31	109	0.499	0.484	0.999	0.980	3640	0.132	2300	0.409
	3.50	2080	30.3	101	.836	.800	.992	.972	7830	.256	4390	.703

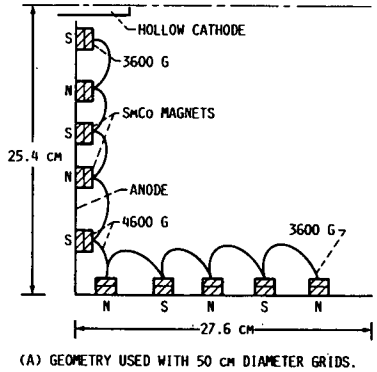

(A) GEOMETRY USED WITH 50 cm DIAMETER GRIDS.

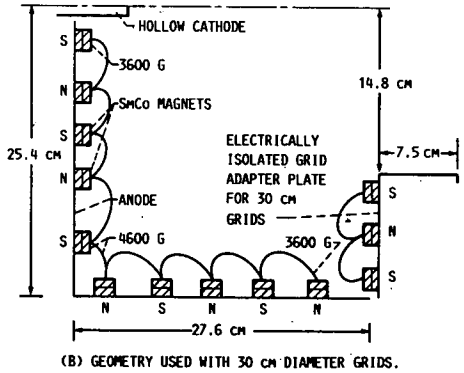

(B) GEOMETRY USED WITH 30 cm DIAMETER GRIDS.

FIGURE 1. - SECTION VIEW OF THE 50 cm DIAMETER RING-CUSP DISCHARGE CHAMBER.

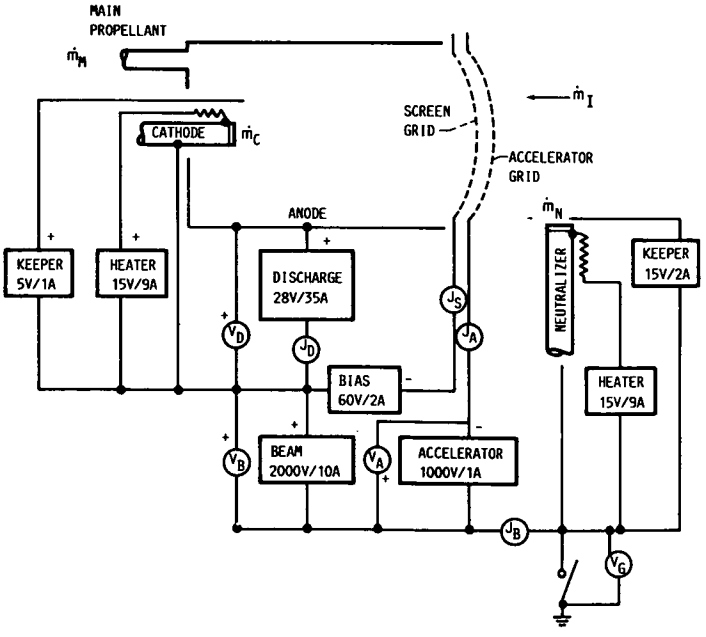

FIGURE 2. - THRUSTER ELECTRICAL SCHEMATIC.

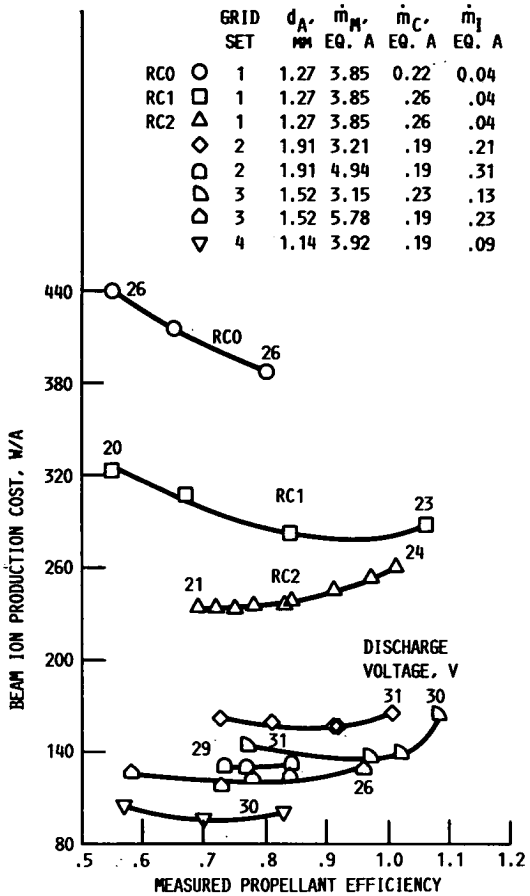

FIGURE 3. - BEAM ION PRODUCTION COSTS AS FUNCTIONS OF PROPELLANT EFFICIENCY FOR 50 cm RING-CUSP THRUSTER WITH 30 AND 50 cm DIAMETER GRIDS.

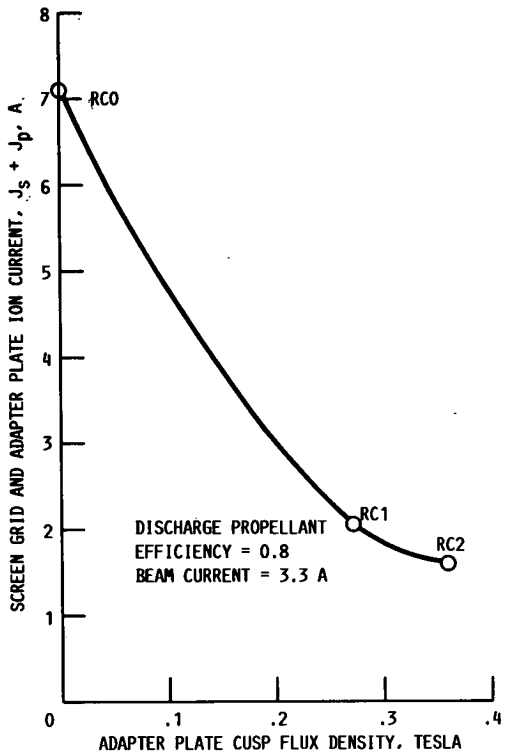

FIGURE 4. - SCREEN GRID PLUS ADAPTER PLATE CURRENT AS A FUNCTION OF ADAPTER PLATE CUSP FLUX DENSITY.

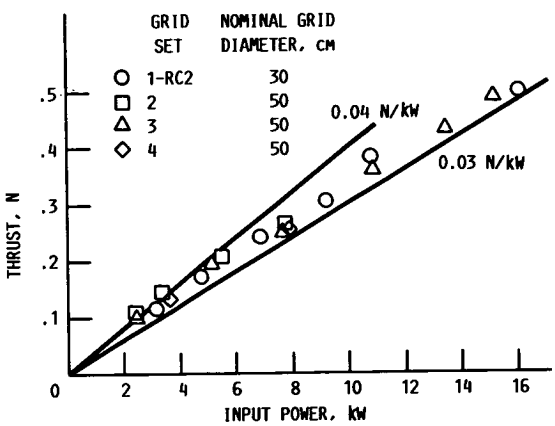

FIGURE 5. - THRUST AS A FUNCTION OF THRUSTER INPUT POWER FOR THE 50 cm DIAMETER RING-CUSP THRUSTER WITH FOUR GRID SETS.

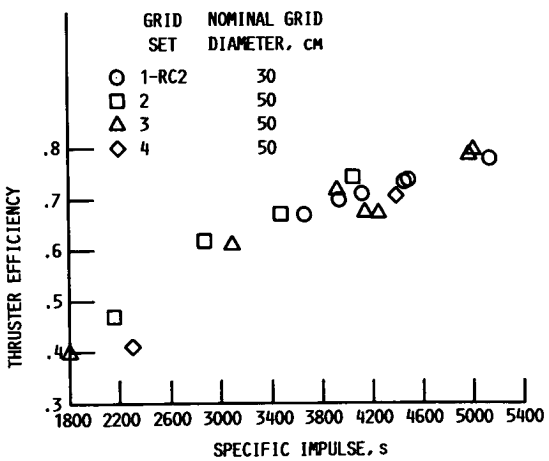

FIGURE 6. - THRUSTER EFFICIENCY AS A FUNCTION OF SPECIFIC IMPULSE, FOR A 50 cm DIAMETER RING-CUSP THRUSTER WITH FOUR GRID SETS.